



Cite this: *RSC Adv.*, 2021, 11, 33798

Synthesized akhtenskites remove ammonium and manganese from aqueous solution: removal mechanism and the effect of structural cations†

Ruifeng Zhang, * Shilian Yang, Chuan Dong, Yu Qiao, Jianmin Zhang and Yingming Guo

Ammonium and manganese removal by tunnel-structured manganese oxide is still enigmatic. Herein, tunnel-structured akhtenskites with different structural cations (Na-MnO_x , Mg-MnO_x , Ca-MnO_x , Fe-MnO_x) were synthesized by the KMnO_4 and Mn^{2+} reaction in the presence of different metal cations, and were used to remove ammonium and manganese from aqueous solution. The results of the batch adsorption experiments indicated that akhtenskites effectively removed NH_4^+ and Mn^{2+} , and the removal process fitted the pseudo-second-order model. By measuring the concentration of nitrate and nitrite, discriminating the adsorbed and oxidized Mn^{2+} , and testing the zeta potential of the oxides, it can be concluded that NH_4^+ was merely removed by electrostatic adsorption *via* $\equiv\text{Mn-O}^-$; Mn^{2+} could also be adsorbed by ion exchange with $\equiv\text{Mn-OH}$, and the adsorbed Mn^{2+} could be partly oxidized. The structural properties of the akhtenskites were characterized by X-ray diffraction (XRD), scanning electron microscopy (SEM), Brunauer–Emmett–Teller (BET) specific area, and X-ray photoelectron spectroscopy (XPS). The experimental results showed that ions with higher valence can result in a higher percentage of Mn(III) in akhtenskite. Mg^{2+} can result in a lower proportion of lattice oxygen in the oxide, and Fe^{3+} can increase the pH of the point of zero charge. Both of them were unfavored for the oxidation of Mn^{2+} . Moreover, it was found that Ca-MnO_x had optimal removal performance in the catalytic oxidation of Mn^{2+} owing to appropriate percentages of O_{latt} and Mn(III) and lower zeta potential. This study provides new insights into the synthesis and application of manganese oxides.

Received 9th August 2021
Accepted 27th September 2021

DOI: 10.1039/d1ra06025b

rsc.li/rsc-advances

1 Introduction

Ammonium and manganese are two important pollutants in water sources in China.¹ Excessive manganese contaminates fabrics, causes esthetic discomfort, and induces central nervous system damage.² Ammonium in water sources can consume dissolved oxygen, increase the amount of disinfectant, and promote the formation of chlorine disinfection byproducts.^{3,4} In addition, both of them often exist simultaneously, making the removal process more complicated.⁵

Several methods have been developed to remove ammonium and manganese from water, such as the addition of oxidants, biological filtration, chemical catalytic oxidation, *etc.*^{6–10} Among these processes, adsorption is one of the most promising strategies due to its high removal efficiency, cost-effectiveness, and easy implementation.^{11–13} The development of new

adsorbents with excellent removal performance is a critical problem to be solved.

Manganese oxide is an important absorbent for removing ammonium and manganese from water because of its low cost, high adsorption capacity, and potential catalytic activity.^{14,15} At present, more than 30 different natural and synthetic manganese oxide minerals are known to exist.¹⁶ Most of them consist of a layer or a tunnel structure with different MnO_6 octahedra arrangements, forming basic building blocks.^{16,17} Manganese oxides are often coated on zeolite, sand, or activated carbon as a filter material.^{12,18} Even in a biofilter, they exhibit a high sorption capacity, which is less dependent on microbial activity.^{19,20}

The removal capability of manganese oxide depends on its structure to some extent.^{21–23} Most studies have focused on layer-structured manganese oxides, such as birnessite.^{10,12,15,23} To the best of our knowledge, there is limited research on tunnel-structured manganese oxide even though it is an important type of manganese oxide.¹⁶ Therefore, more research on the tunnel-structured manganese oxide is necessary. In addition, the fine structure of manganese oxides is vulnerable to factors in the formation environment, such as pH, temperature, aging time, and especially metal ions.²⁴ Metal ions in

School of Urban Planning and Municipal Engineering, Xi'an Polytechnic University, Xi'an, 710048, PR China. E-mail: ruifengzhangtry@xpu.edu.cn; Tel: +86-029-6277-9357

† Electronic supplementary information (ESI) available. See DOI: 10.1039/d1ra06025b



solution could influence the manganese oxide structure by inserting into the interlayer or tunnels in oxides or replacing Mn^{4+} in the MnO_6 octahedral units.²⁵ Unfortunately, few studies have focused on its effects on ammonium and manganese removal.

Compared to other tunnel-structured manganese oxides, akhtenskite ($\epsilon\text{-MnO}_2$) has important applications in the field of environment, although it was discovered relatively late and the structural features are unclear.^{26–28} Therefore, it was selected as a representative and synthesized by a redox reaction between KMnO_4 and MnCl_2 , in the presence of different metal cations (Na^+ , Mg^{2+} , Ca^{2+} , and Fe^{3+}),²⁶ in this study. The aim of this paper is to investigate ammonium and manganese removal capabilities and mechanisms of tunnel-structured manganese oxides and explores the effects of metal ions on the fine structure of the oxide and the removal process.

2 Material and methods

2.1 Manganese oxide preparation

KMnO_4 and $\text{Me}(\text{NO}_3)_n$ (Me represents Na, Mg, Ca, or Fe) were dissolved in 430 mL of deionized water to prepare a 0.1 mol L^{-1} KMnO_4 aqueous solution with $0.37 \text{ mol L}^{-1} \text{Na}^+$ or $0.19 \text{ mol L}^{-1} \text{Ca}^{2+}$, Mg^{2+} , and Fe^{3+} . Then, the KMnO_4 aqueous solution was added dropwise to 345 mL of $0.2 \text{ mol L}^{-1} \text{MnCl}_2 \cdot 4\text{H}_2\text{O}$ under continuous magnetic stirring. The manganese oxide formed was filtered off and washed with deionized water several times until the pH of the cleaning solution was approximately 7.0. Finally, the oxide was dried in an oven for 24 h at $35\text{--}40^\circ\text{C}$ and kept in a sealed container before use.

2.2 Characterization methods

Powder X-ray diffraction (XRD) analysis was performed using a Smartlab9K X-ray diffractometer (Rigaku, Japan) equipped with $\text{Cu K}\alpha$ radiation ($\lambda = 0.1542 \text{ nm}$), operated at 40 kV and 40 mA. Continuous scans were taken in a 2θ range of $5\text{--}80^\circ$ with a scan rate of 5° min^{-1} and a stepwise of 0.02° . SEM images were obtained using a Quanta 600F field-emission scanning electron microscope (FEI incorporation, USA). The binding energies were measured using X-ray photoelectron spectroscopy (XPS) (Thermo Scientific K-Alpha). A conventional $\text{Al-K}\alpha$ anode radiation source was used as the excitation source. The binding energies were calibrated using the C1s binding energy at 284.6 eV. Zeta potential was detected using a Powereach JS94K (Shanghai Zhongchen Digital Technology Equipment Co., Ltd, China). The surface and pore properties of the adsorbent were studied using nitrogen adsorption experiments with an ASAS2020 plus (Micromeritics, USA). The specific surface area of the adsorbent was calculated using the Brunauer–Emmett–Teller (BET) method.

2.3 Removal capability and mechanism evaluation

2.3.1 Adsorption isotherms and kinetics. Kinetics and isotherm experiments were performed in Erlenmeyer flasks in a water bath shaker with a shaking speed of 110 rpm at 25°C . In both experiments, the concentration of Me-MnO_x was 0.5 g L^{-1}

and the reaction solution was 100 mL. Solutions of Mn^{2+} and NH_4^+ were prepared by $\text{MnCl}_2 \cdot 4\text{H}_2\text{O}$ and NH_4Cl , respectively. In the isotherm experiment, the concentrations of Mn^{2+} and NH_4^+ were $5\text{--}25 \text{ mg L}^{-1}$ and $1\text{--}20 \text{ mg L}^{-1}$, respectively, and the equilibration time was 150 min. In the kinetic experiment, the concentrations of Mn^{2+} and $\text{NH}_4^+\text{-N}$ were 25 and 10 mg L^{-1} , respectively, and the samples were taken at 0, 5, 10, 20, 30, 60, and 150 min for detection. Samples for Mn^{2+} and $\text{NH}_4^+\text{-N}$ analysis were obtained by filtration of the suspension through a $0.22 \mu\text{m}$ filter cellulose acetate membrane.

The adsorbed amount of NH_4^+ or Mn^{2+} at time t , $q_t (\text{mg g}^{-1})$, was calculated using eqn (1):

$$q_t = \frac{C_0 - C_t}{m} \times V \quad (1)$$

where $C_0 (\text{mg L}^{-1})$ is the initial concentration of NH_4^+ and Mn^{2+} (mg L^{-1}), C_t is the concentration at time t , $V (\text{L})$ is the volume of the reaction solution, and $m (\text{g})$ is the mass of the adsorbents.

2.3.2 Effect of pH. The removal of Mn^{2+} and NH_4^+ at various pH values was investigated. pH was adjusted in $2.0\text{--}8.0$ by $0.1 \text{ mol L}^{-1} \text{NaOH}$ and $1 \text{ mol L}^{-1} \text{HCl}$ and was. The initial concentrations of Mn^{2+} and $\text{NH}_4^+\text{-N}$ were 25 and 2 mg L^{-1} , respectively. The equilibration time was 150 min.

2.3.3 Simultaneous removal of ammonium and manganese. The concentration of ammonium was 5.0 mg L^{-1} and the concentration of Mn^{2+} was 5.0, 10.0, 15.0 and 25.0 mg L^{-1} , respectively, to study the effect of Mn^{2+} on ammonium removal. The concentration of manganese was 25.0 mg L^{-1} and the concentration of ammonium was 5.0, 10.0 and 15.0 mg L^{-1} respectively to study the effect of ammonium on manganese removal. The equilibrium time was 150 min, and the initial pH was 7.0.

2.3.4 Evaluation of catalytic oxidation capacity. An experiment was designed to determine whether the synthesized oxides had a catalytic oxidation capacity or merely absorption of ammonium and manganese. Two hundred mg L^{-1} of sodium bicarbonate, which is approximate to the alkalinity content in water sources in China,^{9,29} was added to the reaction solution to enhance the acid–base buffer capacity of the reaction system and eliminate the effect of pH. The initial pH of the reaction solution was approximately 8.17.

The catalytic oxidation capacity of ammonium was evaluated by detecting the concentration of nitrate and nitrate produced in the removal process. To investigate the catalytic oxidation of Mn^{2+} , a $50 \text{ mg L}^{-1} \text{Mn}^{2+}$ solution (with $200 \text{ mg L}^{-1} \text{NaHCO}_3$) of 345 mL was added to a sealed glass bottle and reacted with 25 mg Me-MnO_x in a water bath shaker for 600 min. The catalytic oxidation capability of Mn^{2+} was evaluated by discriminating the adsorbed Mn^{2+} and oxidized Mn^{2+} . The amount of total removed manganese (TMn) and the amount of adsorbed manganese (AMn) were detected. AMn was measured as described by Sahabi.¹⁹ When the reaction was complete, the mixture was filtered, and the residual Mn^{2+} in the filtrate was measured. The oxides were collected and washed with deionized water several times. Then, the separated oxide was placed in 100 mL of 10 mM CuSO_4 solution ($\text{pH} = 4.8$) and stored in a closed polyethylene bottle for about 24 h. Since Cu^{2+} can



replace Mn^{2+} on the oxides, any Mn^{2+} adsorbed but not oxidized would be desorbed back into the solution and be detected.

The amount of oxidized manganese (OMn) and the oxidation ratio (OR) were calculated using the following equation:

$$\text{OMn} = \text{TMn} - \text{AMn} \quad (2)$$

$$\text{OR} = \text{OMn}/\text{TMn} \quad (3)$$

2.4 Analytical methods

The chemical reagents used in this study were of analytical grade and purchased from Sinopharm Chemical Reagent Co., Ltd. (Shanghai, China). The pH and dissolved oxygen (DO) were measured using a pH meter (PH-25, Leici Co., China) and dissolved oxygen meter (JPB-607A, Leici Co., China), respectively. The concentrations of Mn^{2+} and NH_4^+ were measured by potassium periodate oxidation spectrophotometry and Nessler's reagent photometry according to the guidelines of the Ministry of Environmental Protection of China.³⁰

3 Results and discussion

3.1 Phase structure of the synthesized manganese oxides

The XRD patterns of the synthesized oxides are shown in Fig. 1. This indicates that all the spectra can be indexed to akhtenskite as compared to the reference pattern ($\epsilon\text{-MnO}_2$, JCPDS 30-0820, $a = 2.80$, $c = 4.45$ Å). The structure of akhtenskite is similar to that of $\gamma\text{-MnO}_2$, but shows more structural faults (De Wolff faults) and microtwinning.^{31,32} The manganese oxide tunnel could be occupied by charge-balancing cations, and the dimensions of the tunnel would vary slightly.^{25,33} This feature highlights the potential of manganese oxides as an adjustable molecular sieve.³⁴ In this study, the experimental results showed that for Na-, Mg-, and Ca- MnO_x , the broad peaks on the left (in the black box) of the spectra were at 21.17° , 20.44° , and 20.78° , respectively. Therefore, the corresponding interplanar spacing was 4.19 Å, 4.34 Å, and 4.27 Å, respectively, according to the Bragg diffraction equation.²⁵ This indicated

that Na^+ , Mg^{2+} , and Ca^{2+} were inserted into the lattice of manganese oxide and changed the tunnel size. For Fe- MnO_x , the intensities of the diffraction peaks of (101), (102), and at the left of the spectrum were weak and eventually disappeared. This suggested that Fe^{3+} made the structure more disordered and the crystalline size of the oxide was smaller.

3.2 Evaluation of removal capability

3.2.1 Adsorption isotherms. The Langmuir and Freundlich model equations are commonly used to describe the adsorption isotherms in water and wastewater treatment.¹² From the adsorption isotherm data, the adsorption capacity or the amount of adsorbent required to remove a pollutant can be obtained. Langmuir and Freundlich data fitting were performed by linearization of eqn (4) and (5), respectively:¹²

$$\frac{C_e}{q_e} = \frac{1}{Kq_{\max}} + \frac{1}{q_{\max}}C_e \quad (4)$$

$$\log q_e = \log K_f + \frac{1}{n} \log C_e \quad (5)$$

where q_e (mg g^{-1}) is the equilibrium adsorption capacity, C_e (mg L^{-1}) is the concentration at equilibrium, q_{\max} ($\text{mg Mn}^{2+}/\text{NH}_4^+-\text{N g}^{-1}$) is the maximum adsorption capacity,

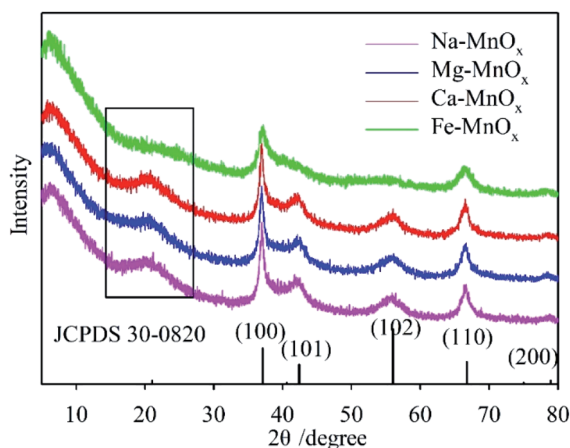


Fig. 1 XRD patterns of the synthesized manganese oxides with different structural cations.

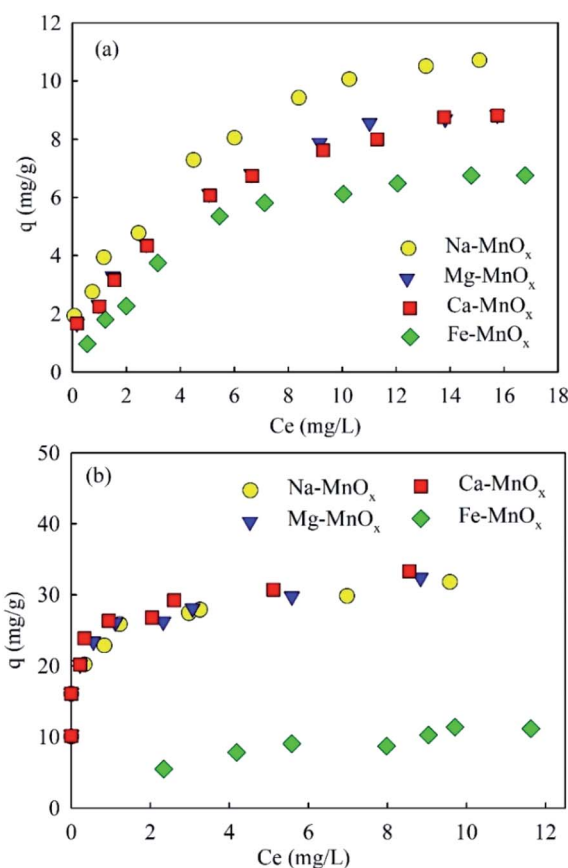


Fig. 2 Ammonium and manganese adsorption isotherms (initial pH for ammonium solution was about 5.0, for manganese was approximately 6.1, adsorbent dose = 0.5 g L^{-1}).



Table 1 Parameters of adsorption isotherms of NH_4^+ adsorption onto MnO_x

Samples	Langmuir model			Freundlich model		
	q_{\max}	k	R^2	K_f	$1/n$	R^2
Na-MnO _x	12.21	0.43	0.972	4.06	0.35	0.946
Mg-MnO _x	10.2	0.38	0.97	3.01	0.41	0.968
Ca-MnO _x	10.1	0.36	0.967	2.93	0.41	0.962
Fe-MnO _x	8.85	0.22	0.988	1.61	0.58	0.955

K ($\text{L mg}^{-1} \text{Mn}^{2+}/\text{NH}_4^+-\text{N}$) is the equilibrium constant, K_F ($\text{mg Mn}^{2+}/\text{NH}_4^+-\text{N g}^{-1} (\text{L mg}^{-1} \text{Mn}^{2+}/\text{NH}_4^+-\text{N})^{1/n}$) is the Freundlich capacity factor, and $1/n$ is the Freundlich intensity parameter.^{12,35}

The adsorption isotherms of the four oxides are shown in Fig. 2. This showed that the performance of Fe-MnO_x was much lower than that of other oxides, especially for manganese removal. The calculated Langmuir and Freundlich parameters related to the adsorption of NH_4^+ and Mn^{2+} are presented in Table 1 and Table 2, respectively. This indicated that both the adsorption process simultaneously fitted the Langmuir and Freundlich model equations well, but the correlation coefficient (R^2) of the Langmuir model equation is higher. According to the Langmuir model, these adsorption processes are preferred for monolayer adsorption.³⁶

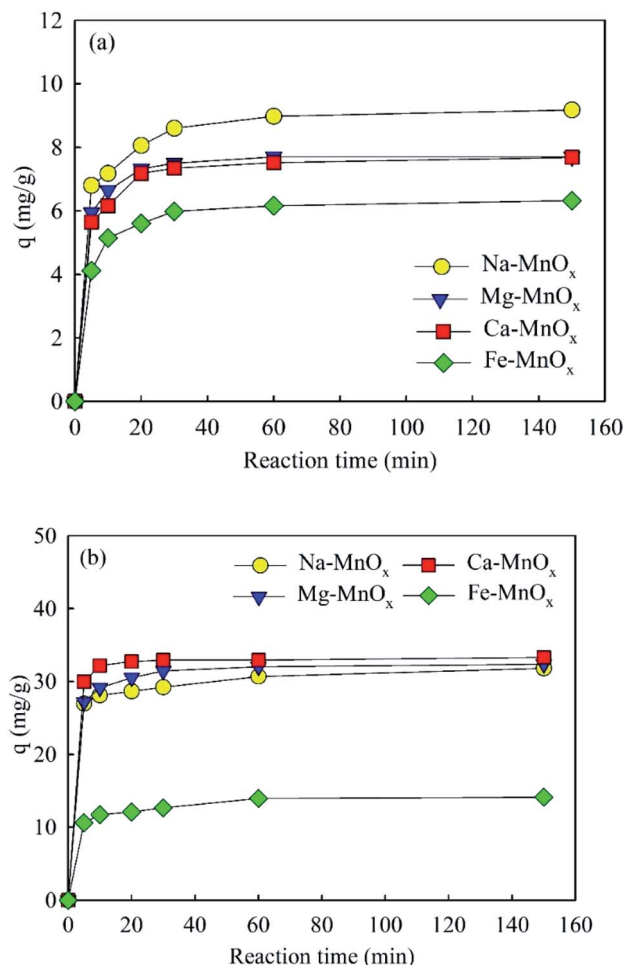
3.2.2 Adsorption kinetics. The adsorption kinetics of NH_4^+ and Mn^{2+} were evaluated using pseudo-first-order and pseudo-second-order kinetic models, respectively. The linear form of the pseudo-first-order kinetic model and pseudo-second-order kinetic model is represented by eqn (6) and (7), respectively:

$$\log(q_{\text{eq}} - q_t) = \log(q_{\text{eq}}) - \frac{K_1 t}{2.303} \quad (6)$$

$$\frac{t}{q_t} = \frac{1}{K_2 q_{\text{eq}}^2} + \frac{1}{q_{\text{eq}}} t \quad (7)$$

where q_{eq} and q_t are the amounts of NH_4^+ or Mn^{2+} adsorbed (mg g^{-1}) at equilibrium and at time t , respectively; K_1 is the Lagergren pseudo-first-order adsorption rate constant (min^{-1}), and K_2 is the pseudo-second-order adsorption rate constant ($\text{g mg}^{-1} \text{min}^{-1}$).^{12,18}

The adsorption amounts as a function of time are shown in Fig. 3. This showed that the adsorption reaction proceeded

**Fig. 3** Adsorption amounts as a function of time: (a) ammonium, (b) manganese (initial pH for ammonium solution was about 5.0, for manganese was approximately 6.1, adsorbent dose = 0.5 g L^{-1} , initial ammonium = 10 mg L^{-1} , initial manganese = 25 mg L^{-1}).

rapidly, especially for manganese removal, which was almost complete in the first 10 min. The calculated parameters of the kinetic models are listed in Tables 3 and 4. This indicated that the kinetic processes of NH_4^+ and Mn^{2+} adsorption agreed well with the pseudo-second-order model. The correlation coefficient R^2 was 0.999, and the fitted q_{eq} approximated the data obtained in the experiment. It appears that the rate-limiting stage in this process could be the chemical adsorption involving valence forces through sharing or exchange of

Table 2 Parameters of adsorption isotherms of Mn^{2+} adsorption onto MnO_x

Samples	Langmuir model			Freundlich model		
	q_{\max}	k	R^2	K_f	$1/n$	R^2
Na-MnO _x	31.55	4.53	0.997	23.2	0.12	0.946
Mg-MnO _x	32.23	5.17	0.995	24.7	0.12	0.968
Ca-MnO _x	33.33	6	0.996	25.6	0.12	0.937
Fe-MnO _x	17.54	0.17	0.949	4.02	0.43	0.946

Table 3 Kinetic constants of NH_4^+ adsorption onto Me-MnO_x

Samples	Pseudo first-order model			Pseudo second-order model		
	K_1	q_{eq}	R^2	K_2	q_{eq}	R^2
Na-MnO _x	0.056	4.29	0.888	0.055	9.26	0.999
Mg-MnO _x	0.113	4.40	0.919	0.129	7.75	0.999
Ca-MnO _x	0.058	3.09	0.818	0.083	7.75	0.999
Fe-MnO _x	0.037	3.08	0.793	0.048	6.49	0.999

Table 4 Kinetic constants of Mn^{2+} adsorption onto Me-MnO_x

Samples	Pseudo first-order model			Pseudo second-order model		
	K_1	q_{eq}	R^2	K_2	q_{eq}	R^2
Na- MnO_x	0.164	9.77	0.654	0.020	32.26	0.999
Mg- MnO_x	0.062	10.47	0.817	0.030	33.33	0.999
Ca- MnO_x	0.058	4.90	0.536	0.078	33.33	0.999
Fe- MnO_x	0.060	7.23	0.908	0.032	14.49	0.999

electrons between adsorbent and adsorbate, based on the assumption of the pseudo-second-order model.¹²

3.2.3 Effect of pH. The adsorption capacity was studied as a function of pH (Fig. 4a). It showed that the adsorption amount of ammonium and manganese increased with the increasing pH. This can be explained by the increased zeta potential and catalytic activity of the oxides, which is significantly influenced by the pH of the aqueous solution.^{20,29} However, when the pH increased to 8.0, the adsorption amount of ammonium decreased. This behavior can be explained by the fact that more

NH_4^+ could be converted into NH_3 species at a pH above 8.0. Similar results have been reported previously for the layer-structured birnessite.¹⁵ Moreover, Fig. 4b shows that when the pH was as low as 2, Mn^{2+} could still be removed. This indicated that Mn in the oxides would not be leached out when the pH was higher than 2.0.

3.2.4 Simultaneous removal of ammonium and manganese. Fig. 5 shows the results of the simultaneous removal of ammonium and manganese. It showed that an increased initial concentration of Mn^{2+} or NH_4^+ could decrease the adsorption amounts of the other ions. This means that the removal processes of these two ions compete with each other. However, a maximum removal capacity of ammonium was also observed at 5 mg L^{-1} , which suggested that a low concentration of Mn^{2+} may promote NH_4^+ removal. It appears that the adsorption sites are relatively adequate at lower concentrations of Mn^{2+} , and when the adsorbed Mn^{2+} is oxidized, it may provide new active sites for ammonium removal. The changes of pH in these experiments are shown in Fig. S1.† In the experiment of ammonium removal at different concentration of Mn^{2+} , the final pH decreased with the increase of the initial concentration

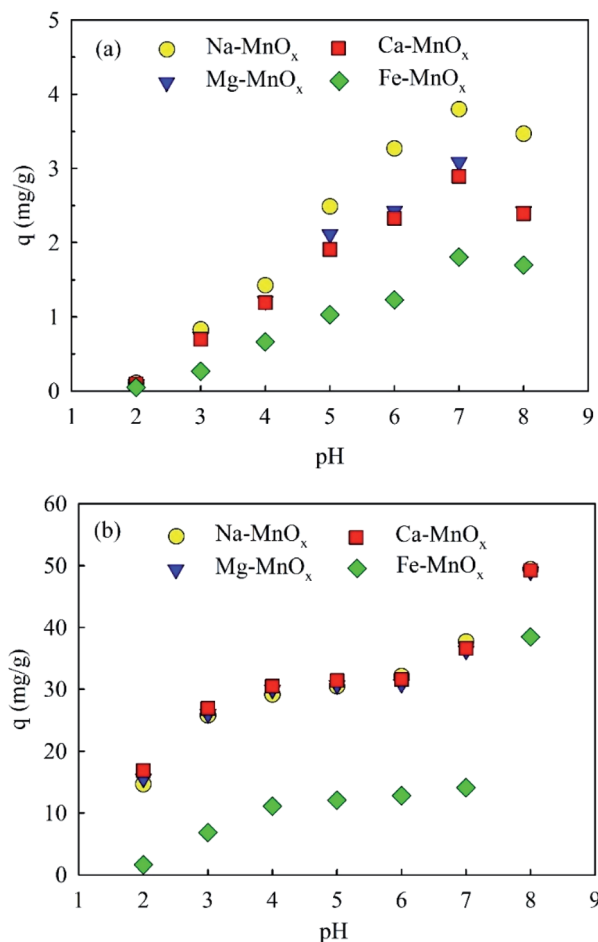


Fig. 4 Effect of pH on (a) ammonium and (b) manganese removal (adsorbent dose = 0.5 g L^{-1} , temperature = 25°C , initial ammonium = 2 mg L^{-1} , initial manganese = 25 mg L^{-1}).

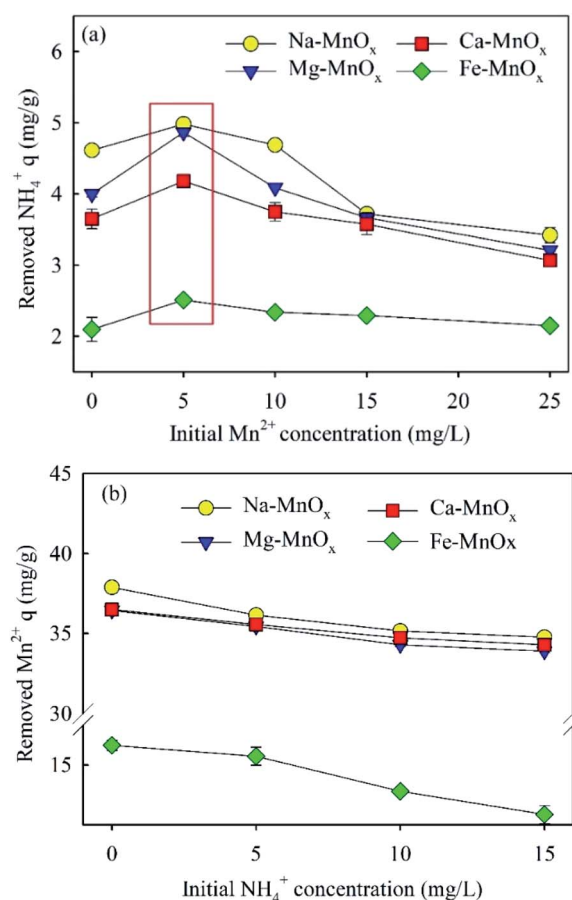


Fig. 5 Performance of the simultaneous removal of ammonium and manganese: (a) ammonium (5 mg L^{-1}) removal at different initial Mn^{2+} concentration; (b) manganese (25 mg L^{-1}) removal at different NH_4^+ concentration (initial pH was approximately 7.0, adsorbent dose = 0.5 g L^{-1}).



of Mn^{2+} . The final pH decreased from 7.49–7.75 (initial $\text{Mn}^{2+} = 0 \text{ mg L}^{-1}$) to 5.55–5.65 (initial $\text{Mn}^{2+} = 25 \text{ mg L}^{-1}$). In the experiment of Mn^{2+} removal at different concentration of NH_4^+ , the final pH increased with the increase of the concentration of NH_4^+ . The final pH increased from 5.48–5.57 (initial $\text{NH}_4^+ = 0 \text{ mg L}^{-1}$) to 5.68–5.82 (initial $\text{NH}_4^+ = 15 \text{ mg L}^{-1}$). The corresponding mechanism is clarified in Section 3.3.3.

3.2.5 Effects of the competent cations present in water. In the treatment of water source, Na^+ , Mg^{2+} and Ca^{2+} may affect the removal of NH_4^+ and Mn^{2+} .^{15,37} In Fig. S2,† it indicates that Na^+ , Mg^{2+} and Ca^{2+} in water have some adverse effects on the adsorption of manganese. The adsorption capacity of Mn^{2+} decreased with the increase of the concentration of Na^+ , Mg^{2+} and Ca^{2+} in water. However, the impact is not significant. The maximum decrease of the adsorption capacity in the four oxides was from 32.7 mg g^{-1} to 29.50 mg g^{-1} (the effect of Mg^{2+} on the Mn^{2+} removal of Na-MnO_x). Different from the removal of manganese, the adsorption capacity of ammonium decreased obviously with the increase of the concentration of Na^+ , Mg^{2+} and Ca^{2+} in water (Fig. S3†). The maximum decrease of the adsorption capacity in the four oxides was from 2.00 mg g^{-1} to 0.89 mg g^{-1} and the adsorption capacity decreased by 55.5% (the effect of Mg^{2+} on the NH_4^+ removal of Ca-MnO_x). It shows that as a monovalent cation, the removal of NH_4^+ is more easily disturbed by other ions in water. In addition, Mg^{2+} has the most significant interference on the removal of ammonium and manganese. It may because of that Mg^{2+} has smaller radius than Ca^{2+} , which results in the stronger electrostatic attraction with MnO_x. Similar results were also found in previous study for the investigation of Na-rich birnessite. Researchers found that Mg^{2+} could increase the surface zeta potential of MnO_x and weaken its surface electronegativity more obviously than Ca^{2+} and Na^+ .¹⁵

3.2.6 Comparison the adsorption capacity with other adsorbents. Table 5 shows the adsorption capacity of some commonly used adsorbents. It indicates that the maximum adsorption capacity of ammonium of akhtenskites is higher than biochar, commercial activated carbon, δ -MnO₂ Coated Zeolite, Greensand and the maximum adsorption capacity of Mn^{2+} is higher than greensand, Fe and Mn oxide-coated sand

and manganese oxide coated zeolite. Consequently, akhtenskites synthesized in this study are promising adsorbents.

3.3 Evaluation of removal mechanism

3.3.1 Morphology and specific surface area. SEM images of the four oxides are shown in Fig. 6. This figure indicates that Na-, Mg-, and Ca-MnO_x consist of spherical particles with pores like a honeycomb or sponge. However, the morphology of Fe-MnO_x was noticeably different, consisting of fine particles. This indicates that structural cations could significantly affect the morphology of manganese oxides. The specific surface area

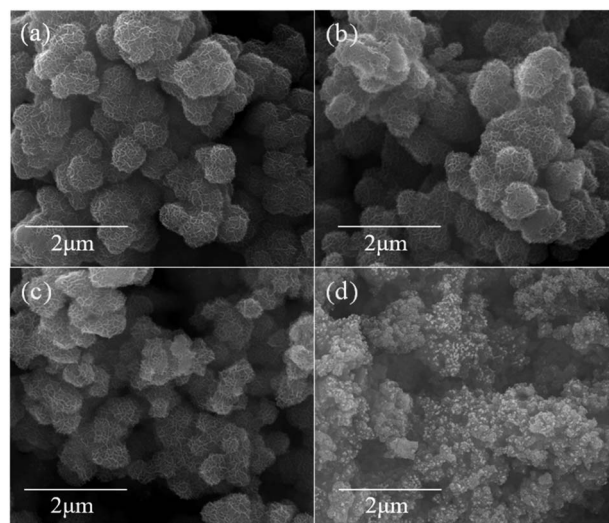


Fig. 6 SEM images of manganese oxides (500 00 \times): (a) Na-MnO_x, (b) Mg-MnO_x, (c) Ca-MnO_x, (d) Fe-MnO_x.

Table 6 Specific surface area (SSA) and pore properties of the oxides

Samples	S_{BET} ($\text{m}^2 \text{g}^{-1}$)	V_{pore} ($\text{cm}^3 \text{g}^{-1}$)	D_{pore} (\AA)
Na-MnO _x	351.05	0.35	39.86
Mg-MnO _x	368.93	0.39	41.92
Ca-MnO _x	400.62	0.38	38.20
Fe-MnO _x	416.86	0.57	54.92

Table 5 The maximum adsorption capacity of some commonly used adsorbents for NH_4^+ and Mn^{2+} removal

Adsorbent	Capacity (mg L^{-1})		Reference
	Ammonium	Manganese	
Biochar	5.86	Not mentioned	38
Commercial activated carbon	0.5	Not mentioned	39
NaOH treated corn cob activated carbon	17.03	Not mentioned	40
δ -MnO ₂ coated zeolite	7.64	23.6	41
Greensand	2.53	11.29	42
Na-rich birnessite	22.61	Not mentioned	15
Fe and Mn oxide-coated sand	Not mentioned	2.617	43
Manganese oxide coated zeolite	Not mentioned	1.123	12
Synthetic manganese oxides	25.77–28.90	Not mentioned	37
Synthesized akhtenskites	8.85–12.21	17.54–33.3	This study

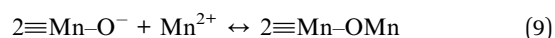
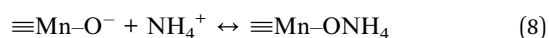


(SSA) and pore properties of the oxides are listed in Table 6. It showed that all the oxides had a high SSA, and that of Fe-MnO_x was the largest. These results differ from those of a previous report on layer-structured birnessite, in which Fe-MnO_x had the minimum specific surface area.²⁵ However, as shown in Fig. 2–5, the capability of Fe-MnO_x was the lowest, although it had the largest SSA and finer particles. It can be derived that the SSA and diameter of the particle are not the most important factors for determining the activity of the oxides. Moreover, it is assumed that zeta potential may be a more important factor, which can affect the removal capability of MnO_x. Further discussion is processed in Section 3.3.2.

3.3.2 Zeta potential and pH changes in the removal process. To explore this mechanism further, the zeta potential of manganese oxide was measured (Fig. 7). This indicated that the point of zero charge (PZC) of Na-, Mg-, and Ca-MnO_x were observed at pH = 2.4–2.7, and that of Fe-MnO_x was measured at pH = 3.5. The results suggested that Fe could increase the PZC of akhtenskite. The adsorption ability of manganese oxide depends on its surface charges to a certain extent.¹⁵ When the pH value is higher than that of PZC, the surface of manganese oxides is negatively charged. It can effectively adsorb NH₄⁺ and Mn²⁺ by electrostatic interactions. Moreover, the amount of negative charge increases with increasing pH. Therefore, this can explain the result of Fig. 4, in which a higher pH corresponds to a higher removal activity. Moreover, the lower removal performance of Fe-MnO_x (Fig. 2–5) could be attributed to the higher zeta potential at pH 2–8, although it had the largest specific surface area (SSA) (Table 6). This indicates that the zeta potential was a more critical factor than SSA to influence the removal activity of manganese oxides. Further, at lower pH, negative charges on the surface of the oxides were less, which weakened the affinity towards NH₄⁺ and Mn²⁺. In addition, increased H⁺ content at lower pH would intensify competition for adsorption sites.^{12,15}

3.3.3 Removal mechanism of adsorption process. Previous research has shown that hydroxyl groups on the surface of manganese oxides are critical for their adsorption capability.^{12,44} In aqueous systems, metal oxides have surface hydroxyl groups that have acidic and basic characteristics simultaneously.¹² When the solution pH is higher than the pH of the PZC, part of

the surface hydroxyl groups on manganese oxides ($\equiv\text{Mn}-\text{OH}$) would change to $\equiv\text{Mn}-\text{O}^-$, and the surface of the oxides was negatively charged.⁴⁵ It is assumed that NH₄⁺ was mainly adsorbed onto $\equiv\text{Mn}-\text{O}^-$, which is a Brønsted base. When NH₄⁺ was adsorbed, the reaction for NH₄⁺ to NH₃ was limited. As a result, the pH of the reaction solution increased. The surface reactions of divalent ions with metal oxide surfaces have been described as the free metal ions exchanged with the H in $\equiv\text{Mn}-\text{OH}$ and formation a hydrolysis complex or abidentate complex.¹² Unlike the removal of NH₄⁺, it can be assumed that Mn²⁺ could also be removed by replacing the H in $\equiv\text{Mn}-\text{OH}$ groups. Thus, the pH of the reaction solution decreased with the removal of Mn²⁺. This hypothesis could be supported by the change in pH in these experiments (Fig. 8). It indicated that pH increased in ammonium removal but decreased in Mn²⁺ removal. The relevant reactions are summarized as follows:



This conclusion is also supported by the results of Fig. 4. When pH = 2, at which the hydroxyl group existed as $\equiv\text{Mn}-\text{OH}$,

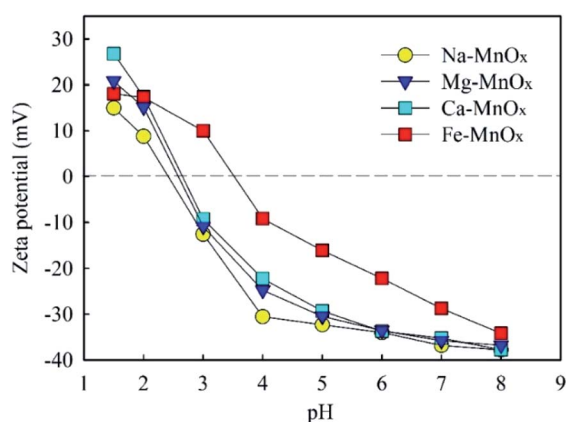


Fig. 7 Zeta potential of manganese oxide as a function of pH.

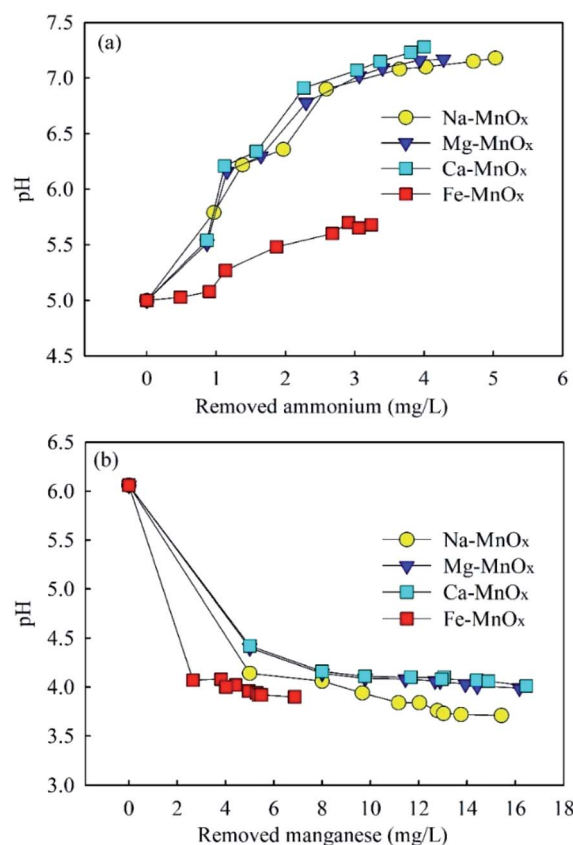


Fig. 8 The changes of pH in (a) ammonium and (b) manganese removal (initial ammonium = 2.0–15.0 mg L⁻¹, initial manganese = 5.0–25.0 mg L⁻¹).



Mn^{2+} could still be removed significantly, but ammonium was hardly removed.

3.3.4 Possible catalytic oxidation activity of the oxides.

Some layer-structured manganese oxides have been reported to remove ammonium and manganese from water by catalytic oxidation.^{9,10} In this study, the possible chemical catalytic oxidation capacity of tunnel-structured akhtenskite was also investigated.

Nitrate and nitrite were measured in the ammonium removal experiment to explore the possible catalytic oxidation of ammonium. The results showed that when ammonium was removed from water, almost no nitrate or nitrite was detected. Therefore, ammonium was merely removed by adsorption. In previous study, researchers also found that Na-rich birnessite synthesized in laboratory, which is layered structure, also removed ammonium just by electrostatic adsorption.¹⁵

The absorbed and oxidized Mn^{2+} in the experiment were measured and calculated, respectively. The results are shown in Fig. 9. This indicated that the akhtenskites could also remove Mn^{2+} by catalytic oxidation. Previous studies suggested that the catalytic oxidation of Mn^{2+} by MnO_x should be a self-catalytic oxidation reaction.^{19,46} In this reaction, MnO_x is not only the catalyst but also the product. The reaction process can be described by the following equation:



As a result, MnO_x is not consumed but produced, so the catalytic reaction can continuously proceed. In addition, Ca- and Mg- MnO_x had the highest and lowest catalytic capacities, respectively. This result is significantly different from the experimental results in Fig. 2–5, in which the activity of Fe- MnO_x was the worst. It has been proven that the catalytic oxidation rates of Mn^{2+} are limited by alkalinity and pH.²⁹ In this study, when $200 \text{ mg L}^{-1} \text{ NaHCO}_3$ was added, the oxidation rate was intensified. Moreover, as shown in Fig. 7, when the pH increased to approximately 8, the zeta potential difference

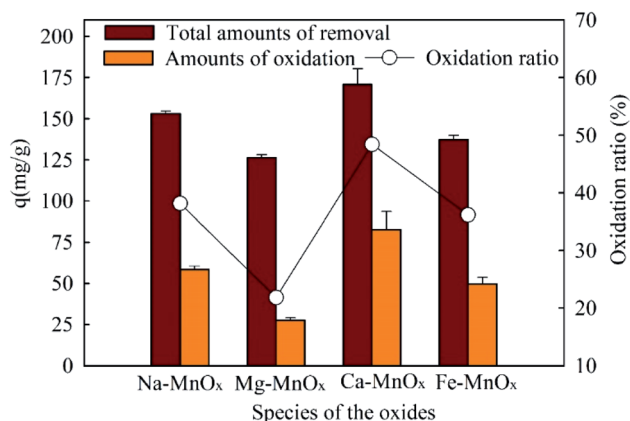


Fig. 9 Amount of oxidized Mn^{2+} in manganese removal by the oxides (dose = 0.07 g L^{-1} , with $200 \text{ mg L}^{-1} \text{ NaHCO}_3$, initial pH = 8.25, manganese = 50 mg L^{-1} , reaction time = 600 min).

between Fe- MnO_x and other oxides was reduced significantly. Therefore, a higher activity of Fe- MnO_x was observed in this stage.

To investigate the manganese oxidation mechanism, XPS profiles were used to identify the species and chemical states of O and Mn present in manganese oxides (Fig. 10). This shows that the O1s spectra could be fitted to three peaks, representing different oxygen species (Fig. 10a). The peaks located at 529.73–530.14, 530.80–531.82, and 532.49–533.41 eV could be attributed to lattice oxygen bonding with Mn (O_{latt}), adsorption of oxygen species (O_{ads}), and oxygen in surface residual water (O_s), respectively.^{21,25} O_{latt} can participate in the oxidation of Mn(II) to Mn(IV), and a higher concentration is favorable for Mn removal.²¹ The atomic percentages of different species of O and Mn are shown in Table 7. It shows that the composition of Mn in different species on the surface of Ca- and Mg- MnO_x is almost the same. However, the proportion of O_{latt} on the surface of Ca- MnO_x is up to 67.2%, which is 44.83% higher than the proportion of Mg- MnO_x (Table 7). In addition, Ca- and Mg- MnO_x have the highest and lowest catalytic capacity, respectively (Fig. 9). Consequently, a higher concentration of surface O_{latt} is favorable for the oxidation of Mn^{2+} . Lattice oxygen has stronger binding force with Mn(II) than the oxygen in water. It

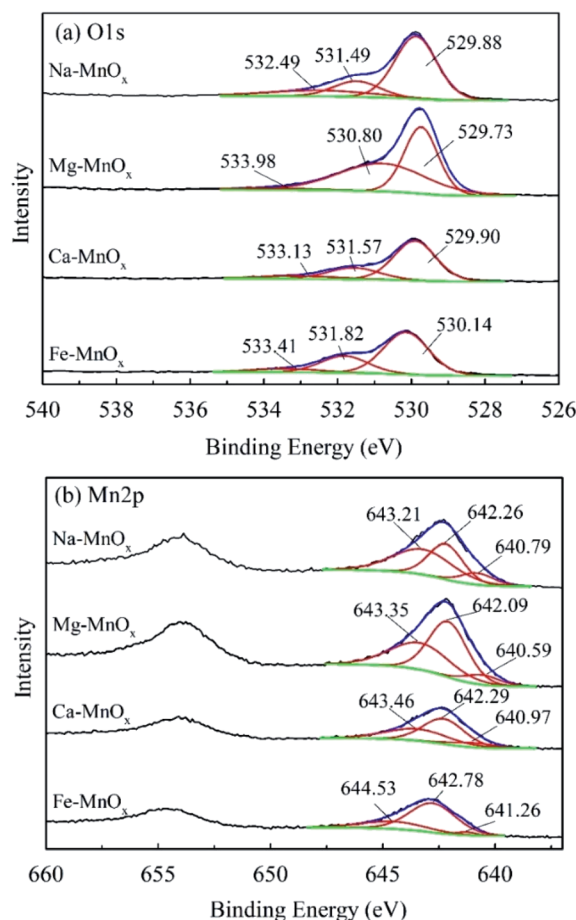


Fig. 10 XPS profiles of O1s and Mn2p in manganese oxides: (a) O1s, (b) Mn2p.

Table 7 Atomic percentage of different species of O and Mn in manganese oxides

Species of the oxides	Species of O (%)			Species of Mn (%)		
	O _{latt}	O _{ad}	O _s	IV	III	II
Na-MnO _x	65.8	18.1	16.1	48.9	38.9	12.8
Mg-MnO _x	46.4	50.4	3.3	39.5	52.2	8.4
Ca-MnO _x	67.2	23.9	8.9	37.6	52.8	9.6
Fe-MnO _x	64.6	27.3	8.0	25.1	71.5	3.4

can react with Mn(II) to form new MnO_x. When the lattice oxygen is consumed it will be reformed by O₂ in water. Similar conclusion had been derived in a manganese oxides filter for the removal of manganese from groundwater.²¹ Moreover, it appears that Mg²⁺ is unfavorable for the formation of O_{latt} in manganese oxide, and the lower O_{latt} content may be the main factor that lowers the catalytic oxidation capability of Mg-MnO_x. However, further studies should be performed to explore how Mg²⁺ can influence the content of O_{latt} in manganese oxides.

Fig. 10b shows that the manganese spectra can also be fitted to three different species. The peaks located at 643.35–644.53, 642.09–642.78, and 640.59–641.26 can be assigned to Mn(IV), Mn(III), and Mn(II), respectively, according to the references in the NIST X-ray Photoelectron Spectroscopy Database. Table 7 shows that the percentage of Mn(III) was the lowest in the monovalent cation doping oxide Na-MnO_x, middle in the divalent cation doping oxides Mg- and Ca-MnO_x and the highest in the trivalent cation doping oxide Fe-MnO_x. This indicates that higher valence cations can induce the formation of more Mn(III) in manganese oxides. Metal cations inside the crystal tunnels can stabilize the negative charge balance originating from Mn(III) in an otherwise perfect Mn(IV)O₂ structure.³⁴ This may be because higher valence ions can balance more negative charges in manganese oxides.

Moreover, Mn(III) is also an important factor affecting the catalytic activity of manganese oxides.^{47,48} Previous research indicated that the superior oxidizing capacity of active MnO_x might arise from the higher Mn(III) content in MnO_x.^{10,22} Mn²⁺ may be removed *via* Mn(III) in the following steps: (1) Mn²⁺ was oxidized by Mn(III) and Mn(III) transferred to Mn(II); (2) Mn(II) was oxidized to Mn(III) by O_{latt}; (3) O₂ in the solution (O₂(aq)) transferred to O_{latt}. In this reaction, Mn(III) was used as a catalyst.

In addition, the Mn(III) content in Fe-MnO_x was the highest, reaching 71.47%. However, its catalytic activity is lower than that of Na-MnO_x and Ca-MnO_x. The reported Mn(III) content of high-activity manganese oxides is commonly 48.4–57.8%.^{10,21} It appears that the high proportion of Mn(III) may not be the best. This may be because of Mn(IV) and vacancy defect in the oxide. The XRD analysis showed that all four MnO_x had poor crystallinity (Fig. 1), which commonly has a high vacancy defect content.⁴⁹ It has been reported that vacancies can act as the active site absorbing Mn²⁺ and the adsorbed Mn²⁺ could be oxidized by Mn(IV) to form Mn(III).²¹ Therefore, the appropriate

Mn(III) content should be dependent on the oxidation rate of Mn²⁺ by different chemical catalytic pathways, which requires further investigation.

To verify these conclusions further, the XPS spectra of the oxides after the reaction of Mn²⁺ removal was detected and shown in Fig. S4.† Different from the results before the reaction, O1s spectra of the oxides after the reaction can only be fitted as two species: O_{latt} and O_{ad}, and O_s was not detected (Fig. S4a†). In addition, the binding energies of different O species decreased. The binding energy of the O_{latt} was 529.55–529.60 eV and the binding energy of O_{ad} was 531.07–531.12 eV. Fig. S4b† shows the Mn2p spectra of the oxides. The binding energies of Mn also decreased after the reaction. According to the fitting results of the Mn2p_{3/2} orbit, Mn can still be fitted into three mixed components. The binding energies at 642.89–643.01 eV, 641.82–641.85 eV and 640.62–640.85 eV represent Mn(IV), Mn(III) and Mn(II) respectively.

Table S1† is the proportion of different species of O and Mn after the reaction. It can be seen that after the reaction, the proportion of Mn(III) (except Fe-MnO_x) and Mn(IV) on the surface of the oxides after reaction decreased significantly, while the proportion of Mn(II) increased. The main reason for the increase proportion of Mn(II) is that the removed Mn²⁺ is just partially oxidized probably. There is a good corresponding relationship between the proportion of Mn(II) and the oxidation rates of Mn²⁺ showed in Fig. 9. While the catalytic efficiency is low, the proportion of Mn(II) on the surface of the oxides is high. The proportion of Mn(II) on the surface of Mg-MnO_x and Ca-MnO_x is the highest (31.84%) and the lowest (21.83%), respectively. It indicates that the Mn²⁺ oxidation rate of Mg-MnO_x is the lowest, and the Mn²⁺ oxidation rate of Ca-MnO_x to is the highest. This conclusion is consistent with the results in Fig. 9.

Further, the ratios of Mn(IV) : Mn(III) before the Mn²⁺ removal reaction are 1.25, 0.76, 0.71 and 0.35 respectively. After the reaction these values are 0.74, 0.85, 0.70 and 1.00, respectively. It shows that Mn(IV) : Mn(III) of Ca-MnO_x is almost unchanged, indicating that its structure is relatively stable. The increased ratio of Mn(IV) : Mn(III) of Fe-MnO_x indicates that Mn(IV) is formed in Mn²⁺ removal process. The relative ratios of Na-MnO_x decreased. It can be derived that Mn(IV) is consumed or Mn(III) is formed in Mn²⁺ removal. These changes further show that the catalytic oxidation process of Mn²⁺ is related to the content of Mn(IV) and Mn(III) in the oxides.

In addition, the lattice oxygen ratio on the oxide surface decreased and the proportion of adsorbed oxygen on the oxide surface increased obviously. No O_s was detected, indicating that the adsorption capability of water of the oxides weakened after the reaction. This may be related to the increase of Mn(II). The decrease of O_{latt} content can be attributed to the consumption of O_{latt} and the decrease of Mn(III) and Mn(IV) content. This further verifies that surface O_{latt} plays an important role in the removal of Mn²⁺.

In summary, Ca-MnO_x had a higher lattice oxygen concentration, more suitable Mn(III) content, and lower zeta potential. These features may be responsible for its higher catalytic oxidation ability. In previous studies, it was thought that Ca had an important effect on the catalytic activity of manganese



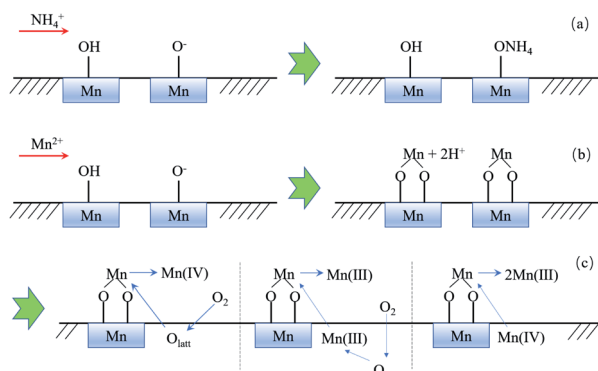


Fig. 11 Removal mechanism of NH_4^+ (a) and Mn^{2+} via MnO_x (b, c).

oxides.^{22,50,51} However, the underlying mechanism is not clear. The experimental results of this study may provide new insights into this question.

3.3.5 Summary of the probable removal mechanism. Based on the analysis of the above experimental results, the removal mechanism of ammonium and manganese can be summarized in Fig. 11. Ammonium is merely removed by electrostatic adsorption with $\equiv\text{Mn}-\text{O}^-$ (Fig. 11a), while Mn^{2+} can be removed by ion exchange with $\equiv\text{Mn}-\text{OH}$ and directly absorbed by $\equiv\text{Mn}-\text{O}^-$ simultaneously (Fig. 11b). Moreover, adsorbed Mn^{2+} can be further catalytically oxidized by three possible pathways (Fig. 11c): (1) being oxidized to Mn(IV) by lattice oxygen directly, and the consumed O_{latt} would be reformed by O_2 in water; (2) being oxidized by Mn(III) and O_{latt} as the final electron acceptor, O_{latt} would also be consumed and reformed by O_2 in water; (3) transferring into Mn(III) via a comproportionation reaction with Mn(IV) . The newly formed oxide is coated on the original oxide surface and produces new surface hydroxyl groups and new lattice oxygen for continuing the removal of ammonium and manganese.

4 Conclusion

In this study, four akhtenskites with different structure cations (Na^+ , Mg^{2+} , Ca^{2+} , Fe^{3+}) were successfully synthesized. The experimental results indicated that the tunnel-structured akhtenskite could remove ammonium and manganese effectively, and the removal performance was significantly affected by pH. NH_4^+ was removed by electrostatic adsorption via $\equiv\text{Mn}-\text{O}^-$. Mn^{2+} could be adsorbed by electrostatic adsorption and ion exchange with $\equiv\text{Mn}-\text{OH}$ simultaneously, and then part of the adsorbed Mn^{2+} could be oxidized catalytically. The structure cations can significantly affect the properties and removal performance of akhtenskite. Higher valence ions can result in higher Mn(III) content in the synthesized manganese oxide. Mg^{2+} reduced the proportion of lattice oxygen in the oxide, and Fe^{3+} can increase the zeta potential of the oxides. Both of them are unfavorable for the oxidation of Mn^{2+} , although Fe^{3+} could also increase the specific area of the oxides. Ca-MnO_x had the optimal removal performance in the catalytic oxidation of Mn^{2+} , which could be attributed to the higher O_{latt} content,

appropriate percentage of Mn(III) , and lower zeta potential. In summary, the synthesized akhtenskites (especially the Ca-MnO_x) are promising adsorbents for the removal of ammonium and manganese from water; in future, researchers can continually explore the regeneration process or strengthen the catalytic capability to further improve the removal capacity and service life of MnO_x .

Author contributions

Ruifeng Zhang, Shilian Yang, Chuan Dong, Yu Qiao, Jianmin Zhang, Yingming Guo work together. Specifically, Ruifeng Zhang was responsible for funding acquisition, data curation and writing; Shilian Yang, Chuan Dong, Yu Qiao were responsible for data curation, investigation and methodology; Jianmin Zhang and Yingming Guo were responsible for data curation and project administration.

Conflicts of interest

There are no conflicts to declare.

Acknowledgements

This work was supported by the Natural Science Basic Research Plan in Shaanxi Province of China (2021JQ-688), and Scientific Research Program Funded by Shaanxi Provincial Education Department, China (No.20JK0656).

Notes and references

- Ministry of Ecology and Environment of China, available online: http://www.mee.gov.cn/home/jrtt_1/201905/t20190529_704841.shtml, 2019.
- J. E. Tobiasson, A. Bazilio, J. Goodwill, X. Mai and C. Nguyen, *Curr. Pollut. Rep.*, 2016, **2**, 168–177.
- A. C. Diehl, G. E. Speitel Jr, J. M. Symons and S. W. Krasner, *Am. Water Works Assoc., J.*, 2000, **92**, 76.
- M. T. Lipponen, M. H. Suutari and P. J. Martikainen, *Water Res.*, 2002, **36**, 4319–4329.
- A. G. Tekerlekopoulou, S. Pavlou and D. V. Vayenas, *J. Chem. Technol. Biotechnol.*, 2013, **88**, 751–773.
- D. Zhang, W. Li, X. Huang, Q. Wen and L. Miao, *Bioresour. Technol.*, 2013, **137**, 147–152.
- F. B. Wagner, P. B. Nielsen, R. Boehansen and H. J. Albrechtsen, *Water Res.*, 2016, **95**, 280–288.
- H. Huang, H. Zhu, W. Gan, X. Chen and X. Yang, *Chemosphere*, 2017, **188**, 257–264.
- Y. Guo, T. Huang, G. Wen and X. Cao, *Chem. Eng. J.*, 2017, **308**, 322–329.
- Y. Cheng, T. Huang, Y. Sun and X. Shi, *Chem. Eng. J.*, 2017, **322**, 82–89.
- J. Huang, N. R. Kankanamge, C. Chow, D. T. Welsh, T. Li and P. R. Teasdale, *J. Environ. Sci.*, 2018, **63**, 174–197.
- S. R. Taffarel and J. Rubio, *Miner. Eng.*, 2010, **23**, 1131–1138.
- S.-H. Pak, C.-G. Park, G. N. Kang and Y.-h. Kim, *Desalin. Water Treat.*, 2018, **123**, 203–210.



- 14 H. Jia, J. Liu, S. Zhong, F. Zhang, Z. Xu, X. Gong and C. Lu, *J. Chem. Technol. Biotechnol.*, 2015, **90**, 1727–1734.
- 15 Y. Cheng, T. Huang, X. Shi, G. Wen and Y. Sun, *J. Environ. Sci.*, 2017, **57**, 402–410.
- 16 J. E. Post, *Proc. Natl. Acad. Sci. U. S. A.*, 1999, **96**, 3447–3454.
- 17 C. M. Santelli, S. M. Webb, A. C. Dohnalkova and C. M. Hansel, *Geochim. Cosmochim. Acta*, 2011, **75**, 2762–2776.
- 18 C. C. Kan, M. C. Aganon, C. M. Futralan and M. L. Dalida, *J. Environ. Sci.*, 2013, **25**, 1483–1491.
- 19 D. M. Sahabi, M. Takeda, I. Suzuki and J.-i. Koizumi, *J. Biosci. Bioeng.*, 2009, **107**, 151–157.
- 20 H. Yang, Z. Yan, X. Du, L. Bai, H. Yu, A. Ding, G. Li, H. Liang and T. M. Aminabhavi, *Chem. Eng. J.*, 2020, **382**, 123033.
- 21 Y. Cheng, T. Huang, C. Liu and S. Zhang, *Chem. Eng. J.*, 2019, **371**, 88–95.
- 22 Y. Cheng, Y. Li, T. Huang, Y. Sun, X. Shi and Y. Shao, *J. Environ. Sci.*, 2018, **65**, 327–334.
- 23 J. H. Bruins, B. Petrusevski, Y. M. Slokar, K. Huysman, K. Joris, J. C. Kruithof and M. D. Kennedy, *Water Res.*, 2015, **69**, 154–161.
- 24 S. Namgung, C.-M. Chon and L. Giehyeon, *Geosci. J.*, 2018, **22**, 373–381.
- 25 J. Wang, D. Li, P. Li, P. Zhang, Q. Xu and J. Yu, *RSC Adv.*, 2015, **5**, 100434–100442.
- 26 M. I. Said, *J. Alloys Compd.*, 2019, 152976.
- 27 Y. J. Shih, R. L. Huang and Y. H. Huang, *J. Cleaner Prod.*, 2015, **87**, 897–905.
- 28 W. Xu, G. Lv, X. Xing, X. J. Zhang and G. S. Wang, *Sci. Adv. Mater.*, 2016, **8**, 966–971.
- 29 X. Tian, R. Zhang, T. Huang and G. Wen, *J. Environ. Sci.*, 2019, **77**, 349–356.
- 30 SEPA, *Analytical Methods of Water and Wastewater*, China Environmental Science Press, Beijing, China, 4th edn, 2002.
- 31 Y.-S. Ding, X.-F. Shen, S. Gomez, H. Luo and S. L. Suib, *Adv. Funct. Mater.*, 2006, **16**, 549–555.
- 32 Y. Liu, H. Wang, Y. Zhu, X. Wang, X. Liu, H. Li and Y. Qian, *Solid State Commun.*, 2009, **149**, 1514–1518.
- 33 Y. Yuan, K. He, B. W. Byles, C. Liu, K. Amine, J. Lu, E. Pomerantseva and R. Shahbazian-Yassar, *Chem*, 2019, **5**, 1793–1805.
- 34 R. Koivula, J. Pakarinen, M. Sivenius, K. Sirola, R. Harjula and E. Paatero, *Sep. Purif. Technol.*, 2009, **70**, 53–57.
- 35 N. Oeztuerk and T. E. Bektas, *J. Hazard. Mater.*, 2004, **112**, 155–162.
- 36 Y. Zheng, J. Zhang and A. Wang, *Chem. Eng. J.*, 2009, **155**, 215–222.
- 37 L. Zhang, J. Wang, H. Qiao, F. Liu and Z. Fu, *J. Cleaner Prod.*, 2020, **272**, 123055.
- 38 X. Zheng, Y. Zhiman, X. Xiaohui, D. Meng and G. Rongbo, *J. Chem. Technol. Biotechnol.*, 2018, **93**, 198–206.
- 39 D. Carey, P. J. Mcnamara and D. H. Zitomer, *Water Environ. Res.*, 2015, **87**, 2098–2106.
- 40 T. V. Mai, H. P. Chao, T. V. Trinh, T. T. Le, C. C. Lin and N. T. Hai, *J. Cleaner Prod.*, 2018, **180**, 560–570.
- 41 W. J. Ma, T. H. Chen, D. Chen, H. B. Liu and Y. Z. Zhang, *Environ. Sci.*, 2019, **40**, 4553–4561.
- 42 A. Mag, A. Sfmk, B. Apa, B. Basa and C. Aam, *Journal of Water Process Engineering*, 2020, **39**, 101714.
- 43 C.-C. Kan, M. C. Aganon, C. M. Futralan and M. L. P. Dalida, *J. Environ. Sci.*, 2013, **25**, 1483–1491.
- 44 Z. W. Han R, Z. Zhang, J. Shi and J. Yang, *J. Hazard. Mater.*, 2006, **137**, 480–488.
- 45 G. Fu, H. E. Allen and C. E. Cowan, *Soil Sci.*, 1991, **152**, 72–81.
- 46 J. Cerrato, W. Knocke, M. Hochella, A. M. Dietrich, A. Jones and T. Cromer, *Environ. Sci. Technol.*, 2011, **45**, 10068–10074.
- 47 M. A. Peluso, L. A. Gambaro, E. Pronato, D. Gazzoli, H. J. Thomas and J. E. Sambeth, *Catal. Today*, 2008, **133**, 487–492.
- 48 G. Wu, Y. Gao, F. Ma, B. Zheng, L. Liu, H. Sun and W. Wu, *Chem. Eng. J.*, 2015, **271**, 14–22.
- 49 Y. Yang, J. Huang, S. Wang, S. Deng, B. Wang and G. Yu, *Appl. Catal., B*, 2013, **142–143**, 567–568.
- 50 M. Wiechen, M. M. Najafpour, S. I. Allakhverdiev and L. Spiccia, *Energy Environ. Sci.*, 2014, **7**, 2203–2212.
- 51 Z. I. Baktash E, M. Schröder, *et al.*, *Dalton Trans.*, 2013, **42**, 16920–16929.

